Ab initio no-core shell model study of $^{10-14}$B isotopes with realistic *NN* interactions

Priyanka Choudhary,[1,*] Praveen C. Srivastava,[1,†] and Petr Navrátil[2,‡]
[1]*Department of Physics, Indian Institute of Technology Roorkee, Roorkee 247667, India*
[2]*TRIUMF, 4004 Wesbrook Mall, Vancouver, British Columbia V6T 2A3, Canada*

(Received 25 July 2020; accepted 21 September 2020; published 8 October 2020)

We report a comprehensive study of $^{10-14}$B isotopes within the *ab initio* no-core shell model (NCSM) using realistic nucleon-nucleon (*NN*) interactions. In particular, we have applied the inside nonlocal outside Yukawa (INOY) interaction to study energy spectra, electromagnetic properties, and point-proton radii of the boron isotopes. The NCSM results with the charge-dependent Bonn 2000 (CDB2K), the chiral next-to-next-to-next-to-leading order (N^{3}LO), and optimized next-to-next-to-leading order (N^{2}LO$_{opt}$) interactions are also reported. We have reached basis sizes up to $N_{\max} = 10$ for ^{10}B, $N_{\max} = 8$ for ^{11,12,13}B, and $N_{\max} = 6$ for ^{14}B with *m*-scheme dimensions up to 1.7×10^9. We also compare the NCSM calculations with the phenomenological YSOX interaction using the shell model to test the predictive power of the *ab initio* nuclear theory. Overall, our NCSM results are consistent with the available experimental data. The experimental ground state spin 3^+ of ^{10}B has been reproduced using the INOY *NN* interaction. Typically, the 3*N* interaction is required to correctly reproduce the aforementioned state.

DOI: 10.1103/PhysRevC.102.044309

I. INTRODUCTION

In nuclear physics, our focus is to describe the nuclear structure including the exotic behavior of atomic nuclei throughout the nuclear chart. The conventional shell model [1–6], where interactions are assumed to exist only among the valence nucleons in a particular model space, is unable to determine the drip line [7,8], cluster structures [9], and halo [10] structures. The study of interactions derived from first principles has been a challenging area of research over the past decades. These fundamental interactions are determined from either meson-exchange theory or quantum chromodynamics (QCD) [11]. QCD is nonperturbative in the low-energy regime, which makes analytic solutions difficult. This difficulty is overcome by chiral effective field theory (χEFT) [12–15]. Chiral perturbation theory (χPT) [16] within χEFT provides a connection between QCD and the hadronic system.

Progress has been made in the development of different many-body modern *ab initio* approaches [17–19], one of them being the no-core shell model (NCSM) [20–31]. *Ab initio* methods are more fundamental compared to the nuclear shell model. The aim of this paper is to explain the nuclear structure of boron isotopes with realistic *NN* interactions as the only input. The well-bound stable nucleus ^{10}B has posed a challenge to the microscopic nuclear theory in particular concerning the reproduction of its ground-state spin [32]. The boron isotopes have been investigated in the past using the shell model [33,34]. The shell model Hamiltonian constructed from a monopole-based universal interaction (V$_{\rm MU}$) in full *psd* model space including (0–3)$\hbar\Omega$ excitations has been used for a systematic study of boron isotopes [33]. This phenomenological effective interaction is obtained by fitting experimental data, thus, it at least partly includes three-body effects. So it is able to reproduce spin of the ground state (g.s.) of ^{10}B. This V$_{\rm MU}$ based Hamiltonian, however, fails to describe the drip line nucleus ^{19}B. The tensor-optimized shell model (TOSM) [34] has been applied to study ^{10}B using the effective bare nucleon-nucleon (*NN*) interaction Argonne V8′ (AV8′) [35]. The g.s. obtained with the AV8′ interaction is 1^+, which, in experiments, is the first excited state of ^{10}B. The AV8′$_{\rm eff}$ interaction, which is a modification of tensor and spin-orbit forces of the AV8′ interaction, gives correct g.s. spin and low-lying spectra, indicating that the tensor forces affect the level ordering. TOSM with the Minnesota (MN) effective interaction [36] without tensor force also gives correct g.s. spin but a smaller g.s. radius compared to the experimental result, which affects the nuclear saturation property, thus providing the small level density.

In Refs. [37–39], the structure of ^{10}B was studied within the NCSM, using accurate charge dependent *NN* potentials up to the fourth order of χPT in basis spaces ($N_{\max}$) of up to $10\hbar\Omega$. Using the *NN* interactions alone led to an incorrect g.s. of ^{10}B. By including the chiral three-nucleon interaction (3*N*), the g.s. was correctly reproduced as 3^+ [37,39]. The *ab initio* NCSM study of ^{10}B with the chiral N^{2}LO (next-to-next-to-leading order) *NN* interaction [40] including three-body forces has been done in Ref. [41], where it was shown that the g.s. energy and spin depend on the chiral order. To correctly reproduce the 3^+ as an experimental g.s., the 3*N* force with the N^{2}LO *NN* interaction is needed. In Ref. [42], the N^{2}LO$_{opt}$

*pchoudhary@ph.iitr.ac.in
†Corresponding author: praveen.srivastava@ph.iitr.ac.in
‡navratil@triumf.ca

interaction was employed in the NCSM calculation for ^{10}B up to $N_{\max} = 10$ ($10\hbar\Omega$) to calculate ground and low-lying excited states. This study reported 1^+ as the g.s. instead of 3^+. Realistic shell model calculations including contributions of a chiral three-body force (N^{3}LO NN + N^{2}LO $3N$ potential) for ^{10}B are reported in Ref. [43]. These results are consistent with the NCSM results with the same interaction. The NCSM with CDB2K potential ($N_{\max} = 8$) and AV8′ ($N_{\max} = 6$) predict 1^+ as the g.s. of ^{10}B [32,44]. The Green's function Monte Carlo (GFMC) approach with AV8′ and AV18 has also been employed to investigate the g.s. of ^{10}B [45], and similarly predicts 1^+ as the ground state with these NN forces.

In Ref. [46], the Daejeon16 and JISP16 (J-matrix inverse scattering potential) NN interactions were applied to p-shell nuclei. For ^{10}B, excitation energies of the 1^+ state with respect to the 3^+ state of 0.5(1) and 0.9(2.4) MeV were reported with Daejeon16 and JISP16 NN interactions, respectively. This means both these NN interactions reproduce the correct g.s. without adding $3N$ forces, but the ordering could not be confirmed on account of the uncertainty in the energy result obtained from the JISP16 interaction.

In recent years, several experimental techniques have been used to measure nuclear charge radius for neutron-rich nuclei towards the drip line [47]. These then serve as a test of the predictive power of *ab initio* calculation. Charge radii inform us about the breakdown of the conventional shell gaps and the evolution of new shell gaps. One of the reasons behind the disappearance of the shell gap is the presence of the halo structure. Tanihata *et al.* [48] measured interaction cross sections (σ_I) for $^{8,12-15}$B using radioactive nuclear beams at the Lawrence Berkeley Laboratory. In this experiment, the interaction nuclear radii and the effective root-mean-square (rms) radii of nucleon distributions were deduced from σ_I. Point-proton radii of $^{12-17}$B were also measured from the charge-changing cross section (σ_{cc}) at GSI, Darmstadt [49]. Further, the proton radii were extracted from a finite-range Glauber model analysis of the σ_{cc}. The measurement shows the existence of a thick neutron surface in ^{17}B [49]. A recent experiment on the nitrogen chain establishes the neutron skin and signature of the $N = 14$ shell gap by measuring proton-radii of $^{17-22}$N isotopes [50].

In the present work, we perform systematic NCSM calculations for $^{10-14}$B isotopes using INOY [51], N^{3}LO [52], CDB2K [53], and N^{2}LO$_{opt}$ [42] NN interactions. For the first time, we report NCSM structure results with the INOY interaction for these isotopes. We have reached basis sizes up to $N_{\max} = 10$ for ^{10}B, $N_{\max} = 8$ for ^{11,12,13}B, and $N_{\max} = 6$ for ^{14}B with m-scheme dimensions up to 1.7×10^9. Apart from energy spectra, we have also calculated electromagnetic properties and point-proton radii. In addition, we compare shell model results of energy levels and nuclear observables obtained with the YSOX interaction [33] with present *ab initio* results.

The paper is organized as follows: In Sec. II, we describe the NCSM formalism. In Sec. III, we briefly review the NN interactions used in our calculations. We present the NCSM results of the energy spectra and compare them to those obtained with the shell model YSOX interaction in Sec. IV. In Sec. V, electromagnetic properties of $^{10-14}$B are reported. In Sec. VI, we discuss point-proton radii of $^{10-14}$B. Finally, we summarize the paper in Sec. VII.

II. NO-CORE SHELL MODEL FORMALISM

In NCSM [27,29], all nucleons are treated as active, which means there is no assumption of an inert core, unlike in the standard shell model. The nucleus is described as a system of A nonrelativistic nucleons which interact by realistic NN or $NN + 3N$ interactions.

In the present work, we have considered only realistic NN interactions between the nucleons. The Hamiltonian for the A nucleon system is then given by

$$H_A = T_{\rm rel} + V = \frac{1}{A}\sum_{i<j}^{A}\frac{(\vec{p}_i - \vec{p}_j)^2}{2m} + \sum_{i<j}^{A} V_{ij}^{NN}, \qquad (1)$$

where $T_{\rm rel}$ is the relative kinetic energy, m is the mass of nucleon, and V_{ij}^{NN} is the realistic NN interaction that contains both nuclear and electromagnetic (Coulomb) parts.

In the NCSM, translational invariance as well as angular momentum and parity of the nuclear system are conserved. The many-body wave function is cast into an expansion over a complete set of antisymmetric A-nucleon harmonic oscillator (HO) basis states containing up to $N_{\max}$ which is HO excitations above the lowest possible configuration.

We use a truncated HO basis while the realistic NN interactions act in the full space. Unless the potential is soft like, e.g., the N^{2}LO$_{opt}$, we need to derive an effective interaction to facilitate the convergence. Two renormalization methods based on similarity transformations have been applied in the NCSM, the Okubo-Lee-Suzuki (OLS) scheme [54–57], and more recently the similarity renormalization group (SRG) [58]. The latter has the advantage of being more systematic and because renormalized potentials are phase-shift equivalent. The three-body induced terms, however, cannot be neglected. Those, in turn, are difficult to converge for potentials that generate strong short-range correlations, such as the CDB2K [59]. The OLS method is applied directly in the HO basis and results in an A- and $N_{\max}$-dependent effective interaction, i.e., the calculation is not variational. The three-body induced terms are less important. It has been observed that the method works particularly well for the INOY interaction [60–63]. Consequently, in this work we apply the OLS method for the INOY, CDB2K, and, for a consistent comparison, also the N^{3}LO NN interaction. For the latter, the SRG method is, however, more appropriate [59,64]. The softer N^{2}LO$_{opt}$ NN interaction is not renormalized.

To facilitate the derivation of the OLS effective interaction, we add the center-of-mass (c.m.) HO Hamiltonian to Eq. (1), which makes the Hamiltonian dependent on the HO frequency:

$$H_{\rm c.m.} = T_{\rm c.m.} + U_{\rm c.m.},$$

where

$$U_{\rm c.m.} = \frac{1}{2}Am\Omega^2\vec{R}^2, \quad \vec{R} = \frac{1}{A}\sum_{i=1}^{A}\vec{r}_i.$$

The intrinsic properties of the system are not affected by the addition of the HO c.m. Hamiltonian due to translational invariance of the Hamiltonian (1).

Thus, we obtain a modified Hamiltonian:

$$H_A^\Omega = H_A + H_{\text{c.m.}} = \sum_{I=1}^{A} h_i + \sum_{i<j}^{A} V_{ij}^{\Omega,A}$$
$$= \sum_{i<j}^{A}\left[\frac{\vec{p}_i^{\,2}}{2m} + \frac{1}{2}m\Omega^2\vec{r}_i^{\,2}\right] + \sum_{i<j}^{A}\left[V_{ij}^{NN} - \frac{m\Omega^2}{2A}(\vec{r}_i - \vec{r}_j)^2\right]. \tag{2}$$

We divide the A nucleon large HO basis space into two parts: one is the finite active space (P) which contains all states up to $N_{\max}$, and the other is the excluded space ($Q = 1 - P$). NCSM calculations are performed in the truncated P space. The two-body OLS effective is derived by applying the Hamiltonian (2) to two nucleons and performing the unitary transformation in the HO basis [27,29]. Eventually, the second term in the brackets in (2) is replaced by the effective interaction.

Finally, we subtract the c.m. Hamiltonian $H_{\text{c.m.}}$ and include the Lawson projection term [65] to shift the spurious c.m. excitations:

$$H_{A,\text{eff}}^\Omega = P\left\{\sum_{i<j}^{A}\left[\frac{(\vec{p}_i - \vec{p}_j)^2}{2mA} + \frac{m\Omega^2}{2A}(\vec{r}_i - \vec{r}_j)^2\right]\right.$$
$$+ \sum_{i<j}^{A}\left[V_{ij}^{NN} - \frac{m\Omega^2}{2A}(\vec{r}_i - \vec{r}_j)^2\right]_{\text{eff}}$$
$$\left. + \beta\left(H_{\text{c.m.}} - \frac{3}{2}\hbar\Omega\right)\right\}P. \tag{3}$$

An extension of the NCSM that provides a unified description of both bound and unbound states is the no-core shell model with continuum (NCSMC) approach [66]. It has been successfully applied, e.g., to explain the parity inversion phenomenon in ^{11}Be [67]. It has not been applied to boron isotopes yet although NCSMC calculations for ^{10,11}B are now in progress.

III. REALISTIC *NN* AND SHELL MODEL INTERACTIONS

In the present work, apart from the INOY interaction [51,68,69], we also report results with the CDB2K [53,70–72], N^{3}LO [11,52], and N^{2}LO$_{opt}$ [42,73] interactions.

The inside nonlocal outside Yukawa (INOY) interaction [51,68,69] has a local character (Yukawa tail) at long distances ($r \geqslant 3$ fm) and a nonlocal one at short distances ($r < 3$ fm), where the nonlocal part is due to the internal structure of the nucleon. As it is constructed in coordinate space, the range of locality and nonlocality is explicitly controllable. This interaction has the form

$$V_{ll'}^{\text{full}}(r, r') = W_{ll'}(r, r') + \delta(r - r')F_{ll'}^{\text{cut}}(r)V_{ll'}^{\text{Yukawa}}(r),$$

where the cutoff function is defined as

$$F_{ll'}^{\text{cut}}(r) = \begin{cases} 1 - e^{-[\alpha_{ll'}(r - R_{ll'})]^2} & \text{for } r \geqslant R_{ll'}, \\ 0 & \text{for } r \leqslant R_{ll'}, \end{cases}$$

and $W_{ll'}(r, r')$ and $V_{ll'}^{\text{Yukawa}}(r)$ are the nonlocal part and the Yukawa tail (the same as in the AV18 potential [74]), respectively. The parameters $\alpha_{ll'}$ and $R_{ll'}$ have the values 1.0 fm^{-1} and 2.0 fm, respectively. Because of the nonlocal character in the INOY interaction, three-body force effects are in part absorbed by nonlocal terms, e.g., it produces correct binding energy of the three-nucleon system (^{3}H and ^{3}He) without adding three-body forces explicitly.

The charge-dependent Bonn 2000 (CDB2K) potential is a meson exchange based potential [53,70–72]. It includes all the mesons with masses below the nucleon mass, i.e., $\pi^{\pm,0}$, η, $\rho^{\pm,0}$, and ω as an exchange particle between nucleons. The η has a vanishing coupling constant, so it can be ignored. This potential also includes two scalar-isoscalar σ (or ϵ) bosons. Charge dependence of nuclear forces, which is investigated by the Bonn full model based on charge independence breaking (difference between proton-proton/neutron-neutron and proton-neutron interactions; pion mass splitting) and charge symmetry breaking (difference between proton-proton and neutron-neutron interactions; nucleon mass splitting) in all partial waves with $J \leqslant 4$ is also reproduced. The potential is represented in terms of the one-boson-exchange (OBE) covariant Feynman amplitudes. The off-shell behavior of the potential, which plays an important role in nuclear structure calculations, is affected by imposing locality on the Feynman amplitudes. So, nonlocal Feynman amplitudes are used in the CDB2K potential. This momentum-space dependent potential fits proton-proton data with χ^2 per datum of 1.01 and the neutron-proton data with χ^2/datum = 1.02 below 350 MeV, where χ^2 is the square of theoretical error over the experimental error.

Chiral perturbation theory is a perturbative expansion in Q/Λ_χ, where $Q \ll \Lambda_\chi \approx 1$ GeV. Entem and Machleidt constructed the *NN* potential [11,52] at fourth order (next-to-next-to-next-to-leading order; N^{3}LO) of χPT in the momentum space. In χPT, two class of contributions determine the *NN* amplitude: contact terms and pion-exchane diagrams. The N^{3}LO interaction contains 24 contact terms, whose parameters contribute to the fit of partial waves of *NN* scattering with angular momentum $L \leqslant 2$. Charge dependence is also included up to next-to-leading order of the isospin-violation scheme. The N^{3}LO has two charge-dependent contacts. Thus, the total number of contact terms is 26. The N^{3}LO has one pion-exchange (OPE) as well as two pion-exchange (TPE) contributions. Contributions of three pion exchange in the N^{3}LO, however, are negligible. OPE and TPE depend on the axial-vector coupling constant g_A (1.29), the pion decay constant f_π (92.4 MeV), and eight low-energy constants (LECs). Three of them (c_2, c_3, and c_4) are varied in the fitting process and the others are fixed. All constants are determined from the *NN* data. With a total of 29 parameters, the N^{3}LO yields χ^2/datum ≈ 1 up to 290 MeV for the fit of neutron-proton data. The accuracy in the reproduction of *NN* data for this order is comparable to the high-precision phenomenological AV18 potential [74].

The N^{2}LO$_{opt}$ [42,73] is a softer interaction and as such, the OLS or SRG renormalization is not needed. This interaction was derived from χEFT at the N^{2}LO order. For the

TABLE I. Dimensions in m-scheme for boron isotopes corresponding to different $N_{\max}$. The dimensions up to which we have reached are shown in blue.

$N_{\max}$	^{10}B	^{11}B	^{12}B	^{13}B	^{14}B
0	84	62	28	5	48
2	1.5×10^4	1.6×10^4	1.2×10^4	6.0×10^3	2.8×10^4
4	5.8×10^5	8.1×10^5	8.4×10^5	6.0×10^5	2.4×10^6
6	1.2×10^7	2.0×10^7	2.5×10^7	2.3×10^7	8.9×10^7
8	1.7×10^8	3.2×10^8	4.7×10^8	5.2×10^8	2.0×10^9
10	1.7×10^9	3.7×10^9	6.3×10^9	8.1×10^9	3.2×10^{10}

optimization of the LECs, the practical optimization using no derivatives (POUNDERs) algorithm was used. In particular, the optimization is performed for the pion-nucleon (πN) couplings (c_1, c_3, c_4) and 11 partial wave contact parameters C and $\tilde{C}$. The N^{2}LO$_{opt}$ interaction reproduces reasonably well experimental binding energies and radii of $A = 3, 4$ nuclei.

For comparison, we have also performed shell model calculations with the phenomenological YSOX interaction [33] developed by the Tokyo group. In the YSOX interaction, ^{4}He is assumed as a core and interactions take place in the *psd* valence space. Single-particle energies are $e_{p_{3/2}} = 1.05$ MeV, $e_{p_{1/2}} = 5.30$ MeV, $e_{d_{5/2}} = 8.01$ MeV, $e_{s_{1/2}} = 2.11$ MeV, and $e_{d_{3/2}} = 10.11$ MeV. There are 516 two-body matrix elements (TBMEs) in this interaction.

NCSM calculations presented in this paper have been performed with the PANTOINE code [75–77]. We have used KSHELL code [78] for the shell model calculation with the YSOX interaction [33]. Recently, we reported NCSM results for N, O, and F isotopes in Refs. [79,80] performed in an analogous way.

IV. RESULTS AND DISCUSSIONS

The dimensions corresponding to different $N_{\max}$ for boron isotopes are shown in Table I. We can see that they increase rapidly with $N_{\max}$ and the mass number. In the present work, we were able to perform NCSM calculations up to $N_{\max} = 10$ for ^{10}B, $N_{\max} = 8$ for ^{11,12,13}B, and $N_{\max} = 6$ for ^{14}B. First, we investigate the dependence on the HO frequency ($\hbar\Omega$) for various $N_{\max}$ bases, typically up to the next to the largest accessible one, for computational reasons. The optimal HO frequency used to calculate the entire energy spectrum is found from the g.s. energy minimum in the largest $N_{\max}$ space. Figure 1 shows variation of g.s. energy of ^{10}B for different basis spaces as a function of HO frequencies for the four

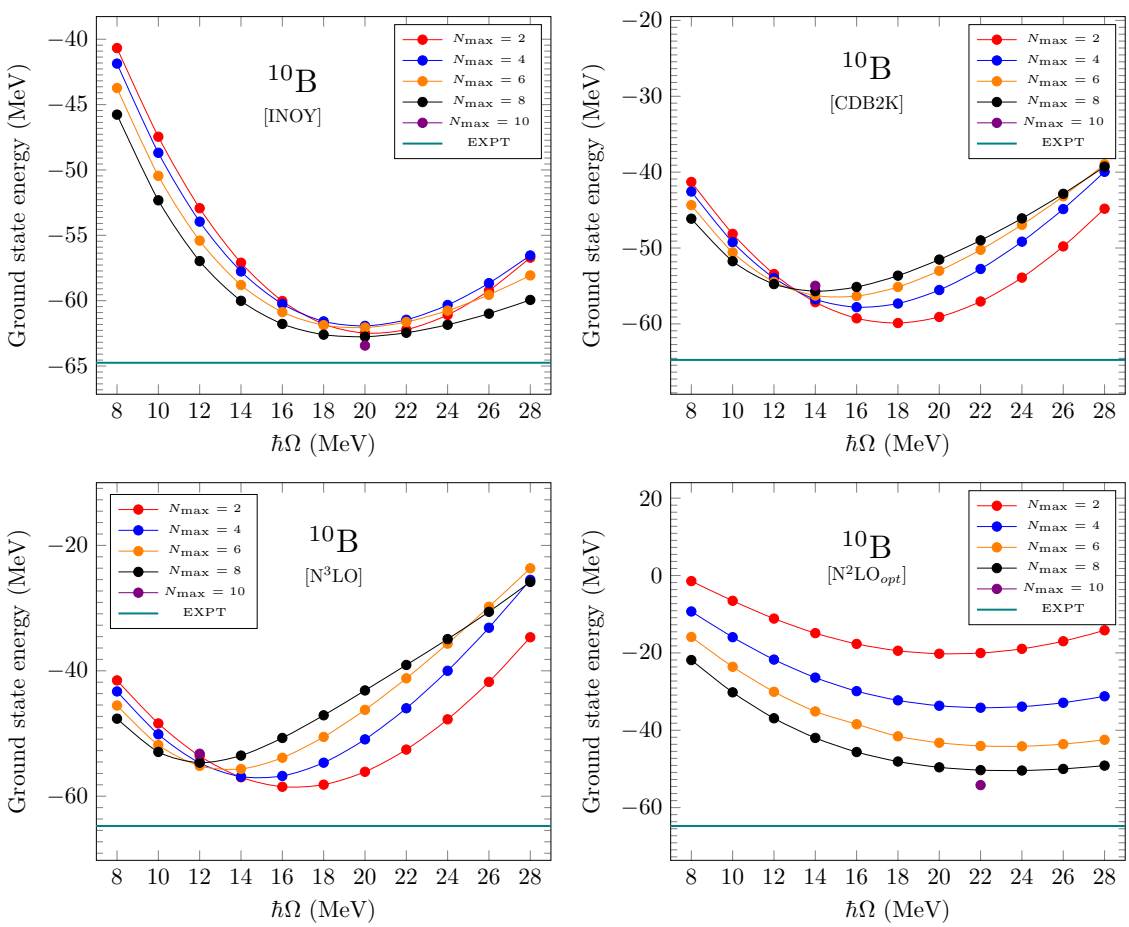

FIG. 1. Ground state energy of ^{10}B as a function of HO frequency for $N_{\max} = 2$ to 10 with the INOY, CDB2K, N^{3}LO, and N^{2}LO$_{opt}$ interactions. Experimental g.s. energy is shown by the horizontal line.

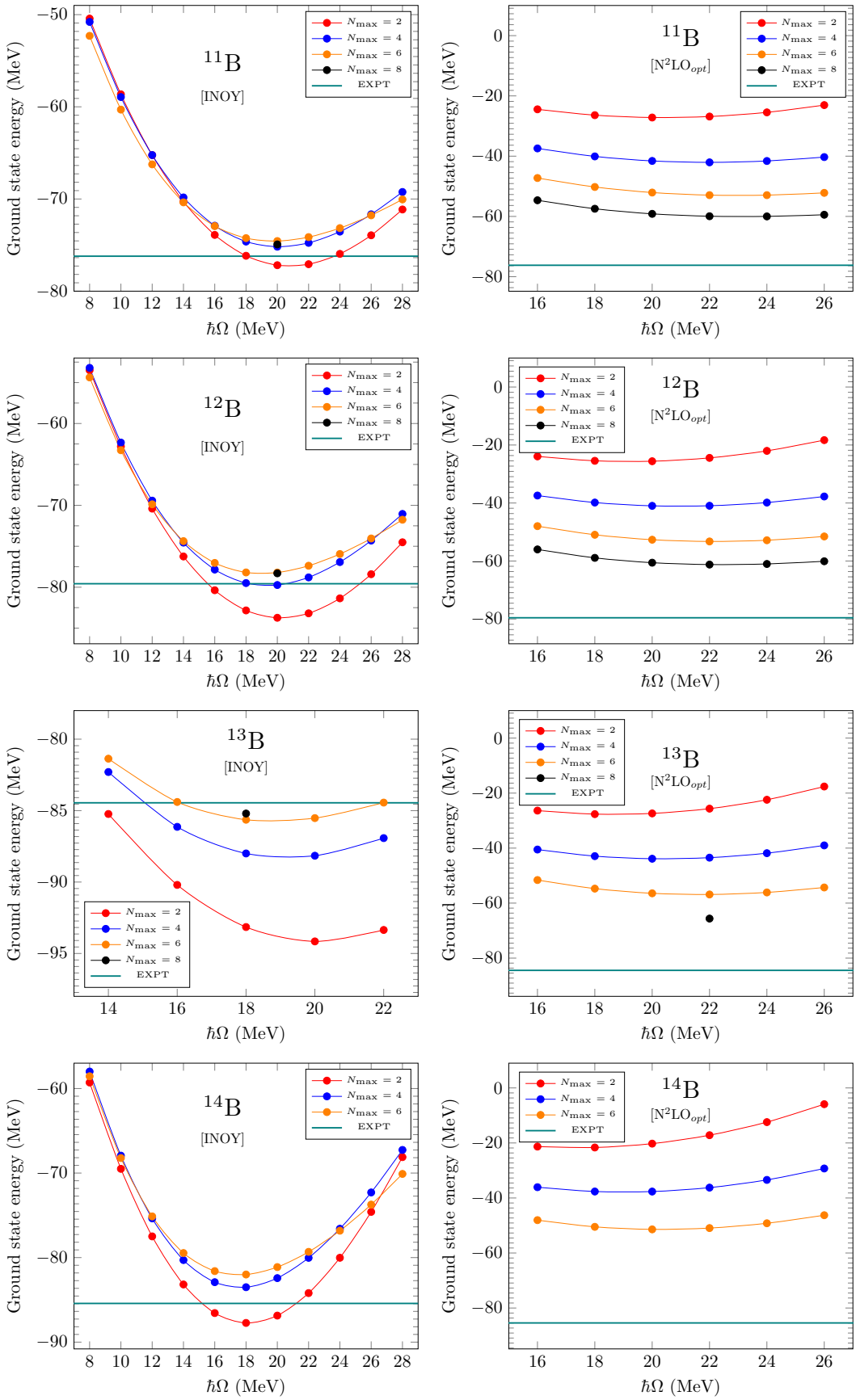

FIG. 2. Ground state energy of ^{11,12,13,14}B as a function of HO frequency for different N_{max} with the INOY and N^{2}LO$_{opt}$ interactions.

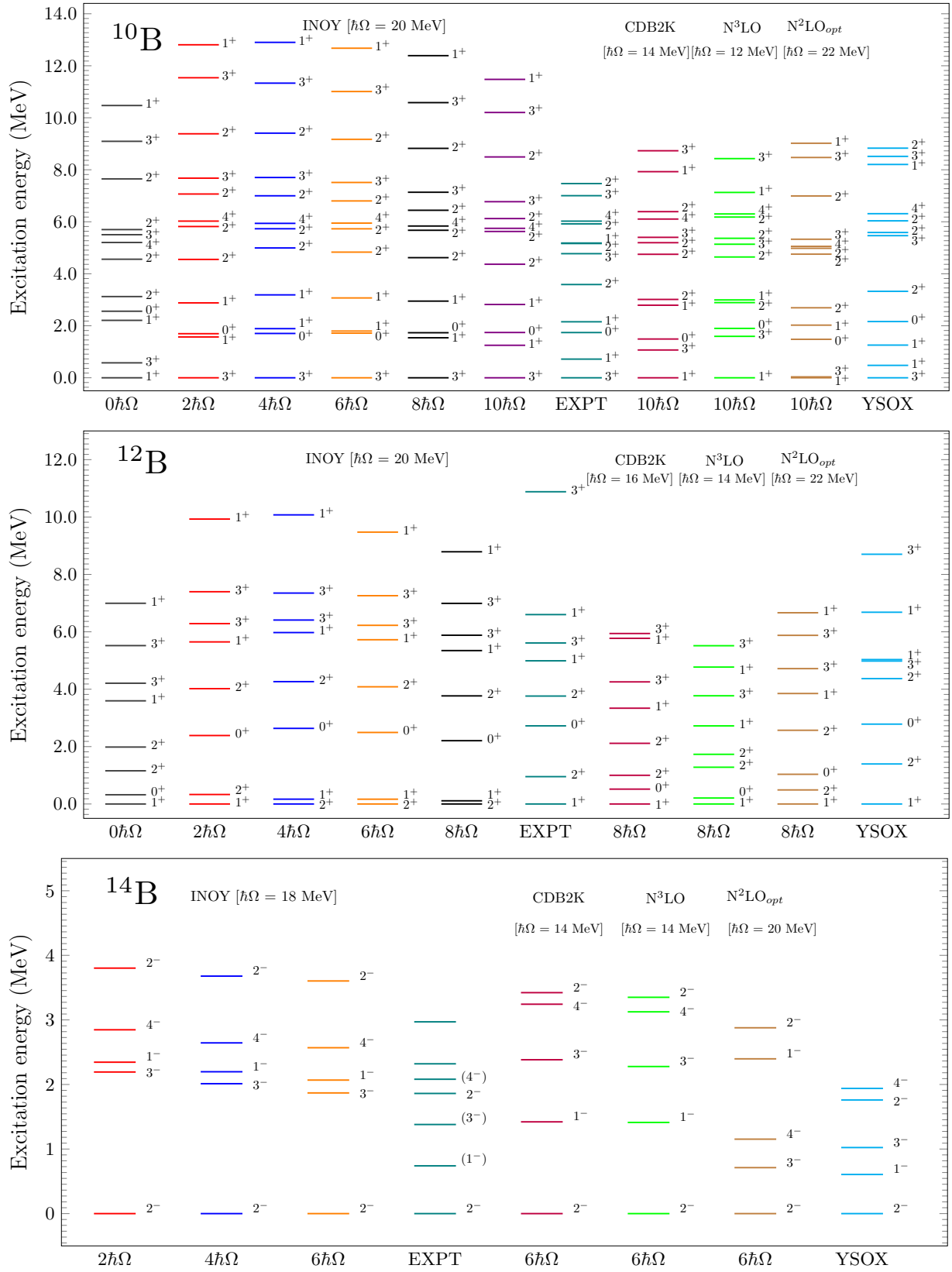

FIG. 3. Comparison of theoretical and experimental energy spectra of ^{10,12,14}B isotopes. The NCSM results are reported with the INOY, CDB2K, N^{3}LO, and N^{2}LO$_{opt}$ interactions at their optimal HO frequencies. Shell model results with the YSOX interaction are also shown.

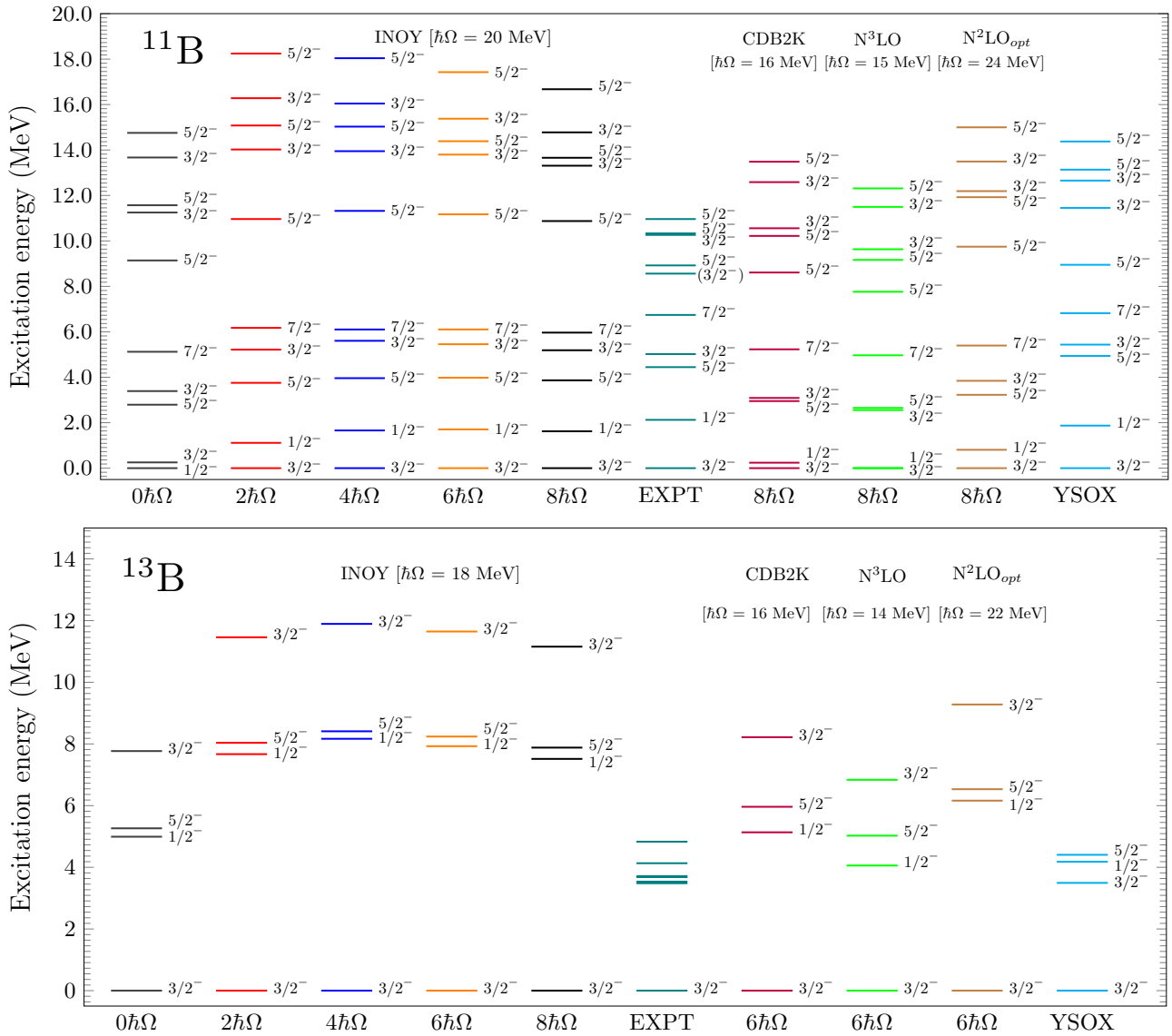

FIG. 4. Comparison of theoretical and experimental energy spectra of ^{11,13}B isotopes. The NCSM results are reported with the INOY, CDB2K, N^{3}LO, and N^{2}LO$_{opt}$ interactions at their optimal HO frequencies. Shell model results with the YSOX interaction are also shown.

interactions that we employ. Overall, we observe a decrease of the g.s. energy dependence on the frequency at higher $N_{\max}$, as expected. Let us reiterate that the N^{2}LO$_{opt}$ calculations are variational while those with the OLS renormalized interactions are not. We note that minima of the g.s. energy are at the same frequency for both $N_{\max} = 6$ and 8 for the INOY interaction. Thus, we expect to obtain the minimum at the same frequency also for $N_{\max} = 10$. Optimal frequency values for the INOY, CDB2K, N^{3}LO, and N^{2}LO$_{opt}$ interactions are at $\hbar\Omega = 20$, 14, 12, and 22 MeV, respectively. We performed the $N_{\max} = 10$ calculations on these frequencies. We have determined the optimal frequencies for other boron isotopes as shown in Fig. 2 corresponding to INOY and N^{2}LO$_{opt}$ interactions. Similarly, we have obtained optimal frequencies for CDB2K and N^{3}LO interactions.

The NCSM results of low-lying states for boron isotopes corresponding to the INOY interaction in the basis spaces $0\hbar\Omega$ to highest $N_{\max}$, and for the other interactions in the highest $N_{\max}$, are shown in Figs. 3 and 4. From the figures, we can see how the energy states approach the experimental values. Along with the NCSM results, we have also reported shell model results corresponding to the YSOX interaction. All results are compared with experimental data. We have calculated only natural parity states for each nucleus.

A. Energy spectra for ^{10,12,14}B

Experimentally, the g.s. of ^{10}B is 3^+ and the first excited state 1^+ lies 0.718 MeV above the g.s. For the INOY interaction, we obtain the correct g.s. 3^+ as seen in the energy spectrum shown in the top panel of Fig. 3. The difference between 3^+ and 1^+ states decreases as $N_{\max}$ increases, and for $N_{\max} = 10$ the difference is 1.250 MeV. Previously, the NCSM results using CDB2K interaction have been reported

TABLE II. Electromagnetic observables of $^{10-14}$B corresponding to the largest $N_{\max}$ at their optimal HO frequencies. Quadrupole moments, magnetic moments, g.s. energies, and $E2$ and $M1$ transitions are in barn (b), nuclear magneton (μ_N), MeV, e^2 fm^4, and μ_N^2 respectively. Experimental values are taken from Refs. [81,82]. YSOX results are also shown for comparison.

^{10}B	Expt.	INOY	CDB2K	N^{3}LO	N^{2}LO$_{opt}$	YSOX
$Q(3^+)$	0.0845(2)	0.061	0.071	0.077	0.067	0.073
$\mu(3^+)$	1.8004636(8)	1.836	1.852	1.856	1.838	1.806
$E_{\text{g.s.}}(3^+)$	−64.751	−63.433	−54.979	−53.225	−54.181	−65.144
$B(E2;3_1^+ \to 1_1^+)$	1.777(9)	0.911	2.091	2.686	1.482	0.757
$B(M1;2_1^+ \to 3_1^+)$	0.00047(27)	0.0007	0.002	0.003	0.0001	0.004
^{11}B	Expt.	INOY	CDB2K	N^{3}LO	N^{2}LO$_{opt}$	YSOX
$Q(3/2^-)$	0.04059(10)	0.027	0.030	0.031	0.029	0.043
$\mu(3/2^-)$	2.688378(1)	2.371	2.537	2.622	2.366	2.501
$E_{\text{g.s.}}(3/2^-)$	−76.205	−74.926	−66.034	−62.915	−59.993	−76.686
$B(E2;7/2_1^- \to 3/2_1^-)$	1.83(44)	0.814	1.258	1.478	1.032	3.118
$B(M1;3/2_1^- \to 1/2_1^-)$	0.519(18)	0.708	0.976	1.051	0.766	0.835
^{12}B	Expt.	INOY	CDB2K	N^{3}LO	N^{2}LO$_{opt}$	YSOX
$Q(1^+)$	0.0132(3)	0.009	0.009	0.010	0.010	0.014
$\mu(1^+)$	1.003(1)	0.561	0.134	0.022	0.282	0.737
$E_{\text{g.s.}}(1^+)$	−79.575	−78.304	−69.350	−68.062	−61.226	−79.264
$B(M1;1_1^+ \to 0_1^+)$	NA	0.047	0.078	0.086	0.066	0.026
$B(M1;2_1^+ \to 1_1^+)$	0.251(36)	0.125	0.197	0.339	0.170	0.204
^{13}B	Expt.	INOY	CDB2K	N^{3}LO	N^{2}LO$_{opt}$	YSOX
$Q(3/2^-)$	0.0365(8)	0.025	0.029	0.031	0.028	0.042
$\mu(3/2^-)$	3.1778(5)	2.844	2.815	2.830	2.781	2.959
$E_{\text{g.s.}}(3/2^-)$	−84.454	−85.205	−75.856	−74.716	−65.624	−84.185
$B(E2;5/2_1^- \to 1/2_1^-)$	NA	1.800	2.281	2.721	1.990	0.787
$B(M1;3/2_1^- \to 1/2_1^-)$	NA	0.984	1.035	1.065	0.982	0.729
^{14}B	Expt.	INOY	CDB2K	N^{3}LO	N^{2}LO$_{opt}$	YSOX
$Q(2^-)$	0.0297(8)	0.016	0.025	0.025	0.004	0.026
$\mu(2^-)$	1.185(5)	0.778	0.926	0.914	0.550	0.614
$E_{\text{g.s.}}(2^-)$	−85.422	−82.002	−76.929	−77.549	−51.413	−84.454
$B(M1;2_1^- \to 1_1^-)$	NA	2.579	2.457	2.436	2.755	2.656

for $N_{\max} = 8$ [44]. In the present paper, we have extended the basis size from $N_{\max} = 8$ to 10 to further improve convergence. Overall, the present results are consistent with those of Ref. [44]. The CDB2K interaction is unable to reproduce the correct g.s. 3^+. For comparison, we have also studied NCSM results with N^{3}LO and N^{2}LO$_{opt}$ interactions for $N_{\max} = 10$. These interactions predict 1^+ as the g.s. contrary to the experimental result, albeit the difference between 3^+ and 1^+ states is very small (0.035 MeV) for the N^{2}LO$_{opt}$ interaction. We note that the calculated 3_1^+ results corresponding to CDB2K and N^{3}LO interactions are, respectively, 1.069 and 1.594 MeV above the 1_1^+ state. We can also see that the INOY interaction predicts the correct ordering of 3^+-1^+-0^+-1^+-2^+ states, contrary to the phenomenological YSOX interaction.

As seen in the second panel of Fig. 3, the INOY interaction fails to predict correct g.s. 1^+ for ^{12}B, while CDB2K, N^{3}LO, and N^{2}LO$_{opt}$ interactions are able to predict the g.s. correctly. At the same time, it is clear that the difference between 1^+ and 2^+ states decreases with increasing $N_{\max}$ for the INOY interaction. So, we expect that for larger $N_{\max}$ the g.s. would be 1^+ also for the INOY interaction. Using CDB2K and N^{3}LO interactions, the NCSM results are too compressed compared to experimental results. In particular, the 0^+ state is too low. The N^{2}LO$_{opt}$ interaction gives the correct order of the energy levels up to 3_1^+ with lower energy values than the experimentally obtained energies.

For ^{14}B, we have reached only $N_{\max} = 6$ space, due to huge dimensions of the Hamiltonian matrix involved in the calculation. All interactions provide the correct g.s. as 2^-. Experimentally, 1_1^- and 3_1^- states are tentative, which are confirmed with the CDB2K and N^{3}LO interactions. These states are also confirmed with YSOX interaction. For the INOY interaction, the order of states 1_1^-, 3_1^- and 2_1^-, 4_1^- is reversed in comparison to the (tentative) experimental data. The energy difference between 2_1^- and 1_1^- states is larger for all *ab initio* interactions compared to that obtained in experiment.

B. Energy spectra for ^{11,13}B

For ^{11}B, we employed HO frequencies of 20, 16, and 24 MeV for the INOY, CDB2K, and N^{2}LO$_{opt}$ interactions, respectively. For the N^{3}LO interaction, the optimal frequency is taken to be 15 MeV from Ref. [37]. The $3/2^-$ state is the experimental g.s. of ^{11}B. Our NCSM calculations reproduce the correct g.s. with all four interactions. We get correct excited states up to ≈ 7 MeV with all interactions except the N^{3}LO. The experimental g.s. energy of the $3/2^-$ state is −76.205 MeV. With the INOY interaction, we obtain the energy of

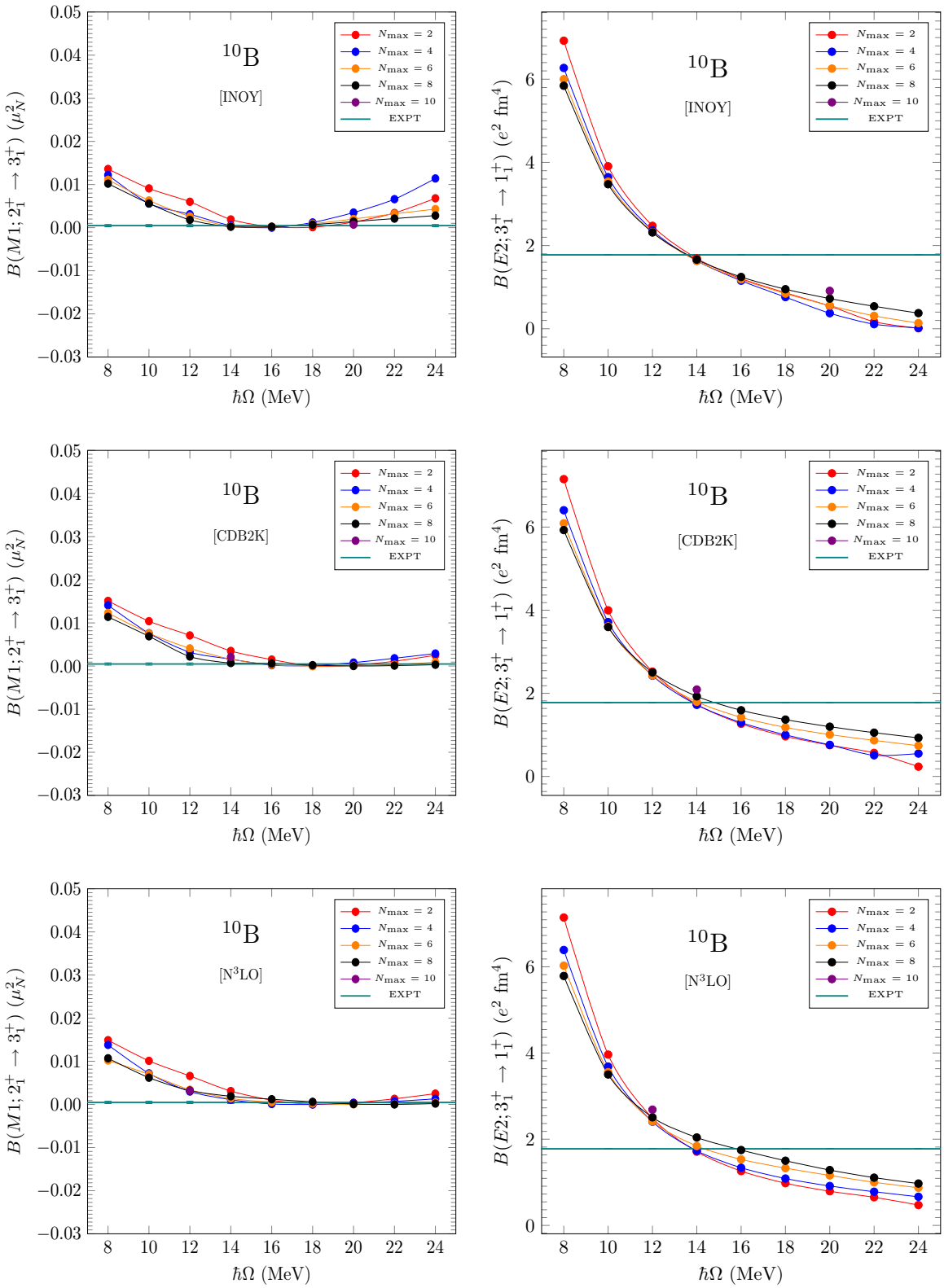

FIG. 5. Variation of B(M1:$2_1^+ \to 3_1^+$) and B(E2:$3_1^+ \to 1_1^+$) for ^{10}B with HO frequency for $N_{\max} = 2$ to 10, corresponding to the INOY, N^{3}LO and CDB2K interactions. Experimental values are shown by horizontal line with uncertainty.

-74.9 MeV for this state, fairly close to the experimental value. For the N^{3}LO interaction, $3/2^-$ and $1/2^-$ states are almost degenerate, while the INOY gives a splitting close to experimental. This splitting depends on the strength of the spin-orbit interaction, which is apparently the largest for the INOY interaction. We note that the energy gap between

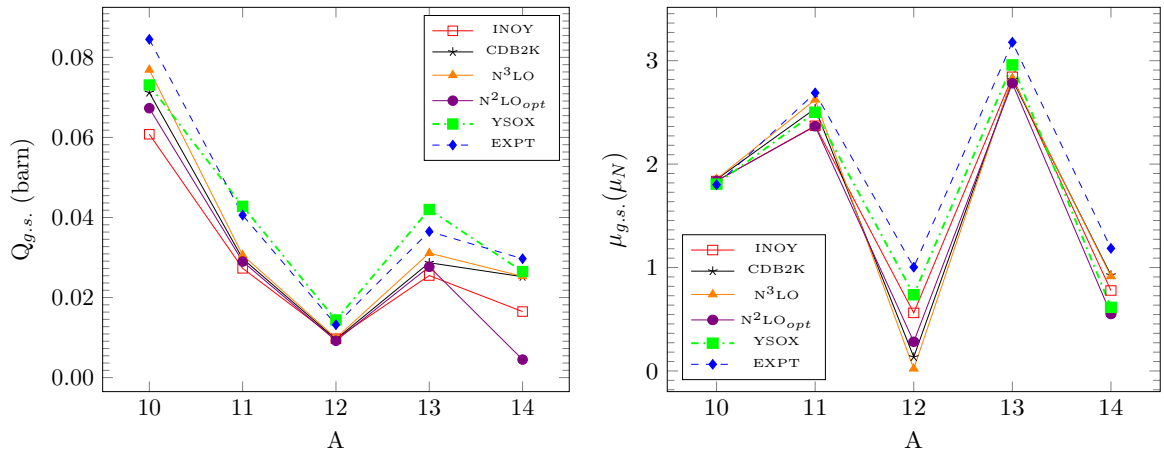

FIG. 6. Ground state quadrupole and magnetic moment dependencies on the mass number of the studied boron isotopes. NCSM results obtained at the largest accessible $N_{\max}$ space with the optimal frequency are shown. Experimental values are taken from Ref. [82].

the states $7/2_1^-$ and $5/2_2^-$ obtained using the INOY interaction is very large compared to the experimental value. This could be because the optimal HO frequency is chosen with respect to the g.s. which is then used to predict the whole energy spectrum. It is possible that a faster convergence of the excited states could be achieved with a different optimal frequency. Our NCSM calculations have been performed up to $N_{\max} = 8$ for ^{13}B, for which we obtain the correct g.s. with all interactions. The energy difference between theoretical and experimental excited states is rather large, which makes it difficult to use the present calculations for assigning experimentally unknown spin and parity to the excited states.

V. ELECTROMAGNETIC PROPERTIES

Table II contains quadrupole moments (Q), magnetic moments (μ), g.s. energies ($E_{\text{g.s.}}$), reduced electric quadrupole transition probabilities [$B(E2)$], and reduced magnetic dipole transition probabilities [$B(M1)$]. Only one-body electromagnetic operators were considered. The experimental binding energy of ^{10}B is -64.751 MeV. The INOY interaction underbinds the ^{10}B nucleus by 1.32 MeV while the YSOX interaction overbinds this by 0.39 MeV. The other realistic interactions we used underestimate the experimental binding energy more significantly. The g.s. Q and μ moments of ^{10,11}B are in a reasonable agreement with experiment for all interactions. On the other hand, the calculated $B(E2; 3_1^+ \to 1_1^+)$ value for ^{10}B varies substantially. Similarly, we find interaction dependence and stronger disagreements with experiment for the ^{12,13,14}B g.s. moments. We predict several $B(E2)$ and $B(M1)$ values for $^{12-14}$B which are not yet measured experimentally. In Fig. 5, we show $B(M1; 2_1^+ \to 3_1^+)$ and $B(E2; 3_1^+ \to 1_1^+)$ transition strengths corresponding to different $N_{\max}$ and $\hbar\Omega$ for ^{10}B with the INOY, CDB2K, and N^{3}LO interactions. $B(M1; 2_1^+ \to 3_1^+)$ curves become flat, which means they become independent of $N_{\max}$ and $\hbar\Omega$. So, the convergence of the $B(M1)$ result is obtained at smaller $\hbar\Omega$ and lower $N_{\max}$. As discussed, e.g., in Refs. [30,31], it is a big task to compute the $E2$ transition operator, as it depends on the long-range correlations in the nucleus, i.e., the tails of nuclear wave functions. From Fig. 5, we can see that $B(E2)$ value varies even for large value of the $N_{\max}$ parameter. The best $B(E2)$ value is then taken where these curves become flat, although clearly we have not reached convergence within the model spaces used in this work.

The quadrupole and magnetic moments of the studied isotopes are summarized in Fig. 6. Overall, the experimental trends are well reproduced for both observables although the NCSM calculations systematically under predict the experimental quadrupole moments.

In Fig. 7, the dependence of the calculated g.s. energies on the mass number of boron isotopes is plotted with INOY, CDB2K, N^{3}LO, N^{2}LO$_{opt}$, and YSOX interactions and compared with experimental energies. NCSM results obtained at the largest accessible $N_{\max}$ space with the optimal frequency

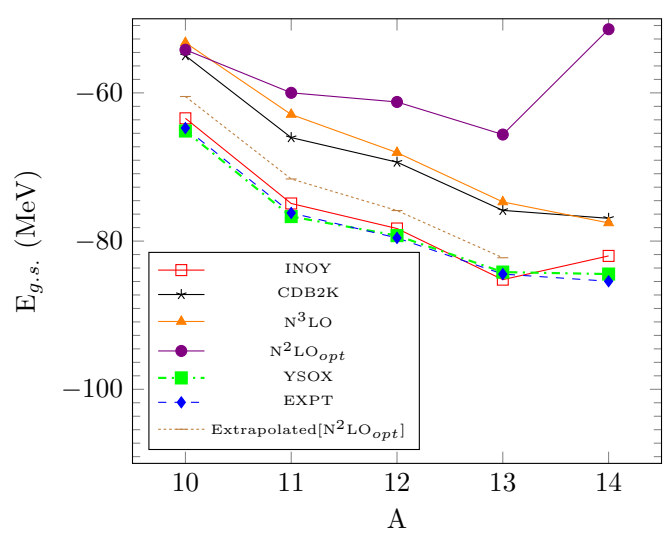

FIG. 7. Dependence of the calculated g.s. energies on A of boron isotopes with INOY, CDB2K, N^{3}LO, N^{2}LO$_{opt}$, and YSOX interactions and compared with experimental energies. NCSM results obtained at the largest accessible $N_{\max}$ space with the optimal frequency are shown.

TABLE III. Calculated point-proton radii (r_p) of $^{10-14}$B with INOY, CDB2K, and N^{3}LO interactions at highest $N_{\max}$ corresponding to their optimal HO frequencies. Experimental point-proton radii are taken from Ref. [49]. The point-proton radii are given in fm.

r_p	Expt.	INOY	CDB2K	N^{3}LO
^{10}B	2.32(5)	2.03	2.27	2.38
^{11}B	2.21(2)	1.97	2.15	2.24
^{12}B	2.31(7)	1.96	2.13	2.23
^{13}B	2.48(3)	1.98	2.10	2.20
^{14}B	2.50(2)	1.99	2.18	2.20

are shown. From Fig. 7, we can conclude that INOY interaction provides a better description for g.s. energy than the other *ab initio* interactions we used.

For the N^{2}LO$_{opt}$ interaction, we have extrapolated the g.s. energy using an exponential fitting function $E_{\text{g.s.}}(N_{\max}) = a\exp(-bN_{\max}) + E_{\text{g.s.}}(\infty)$, with $E_{\text{g.s.}}(\infty)$ the value of g.s. energy at $N_{\max} \rightarrow \infty$. In particular, we have used the last three $N_{\max}$ points in the extrapolation procedure. For ^{14}B, no meaningful extrapolation was possible.

VI. POINT-PROTON RADII

In Table III, we have presented point-proton radii (r_p) using NCSM with INOY, CDB2K, and N^{3}LO interactions at their optimal frequencies along with experimentally observed radii [49]. The INOY interaction considerably underestimates the radii. For ^{10,11}B, the CDB2K and N^{3}LO interactions produce better results, with the former slightly underestimating and the latter slightly overestimating the radii. For $^{12-14}$B, the radii are underestimated for all interactions.

In Fig. 8, we present the variation of ^{10}B r_p with frequency and $N_{\max}$ for INOY, CDB2K, and N^{3}LO interactions. With the enlargement of basis size $N_{\max}$, the dependence of r_p on frequency decreases. The curves of r_p corresponding to different $N_{\max}$ intersect each other approximately at the same point. We take this crossing point as an estimate of the converged radius [46,83]. In particular, we consider the intersection point of the curves at the highest successive $N_{\max}$ as an estimate of the converged radius. In this way, we obtain ^{10}B point-proton radii for INOY, CDB2K, and N^{3}LO interactions 2.14, 2.30, and 2.36 fm, respectively.

Similarly, we have shown variation of r_p with frequency and $N_{\max}$ for other isotopes corresponding to the INOY

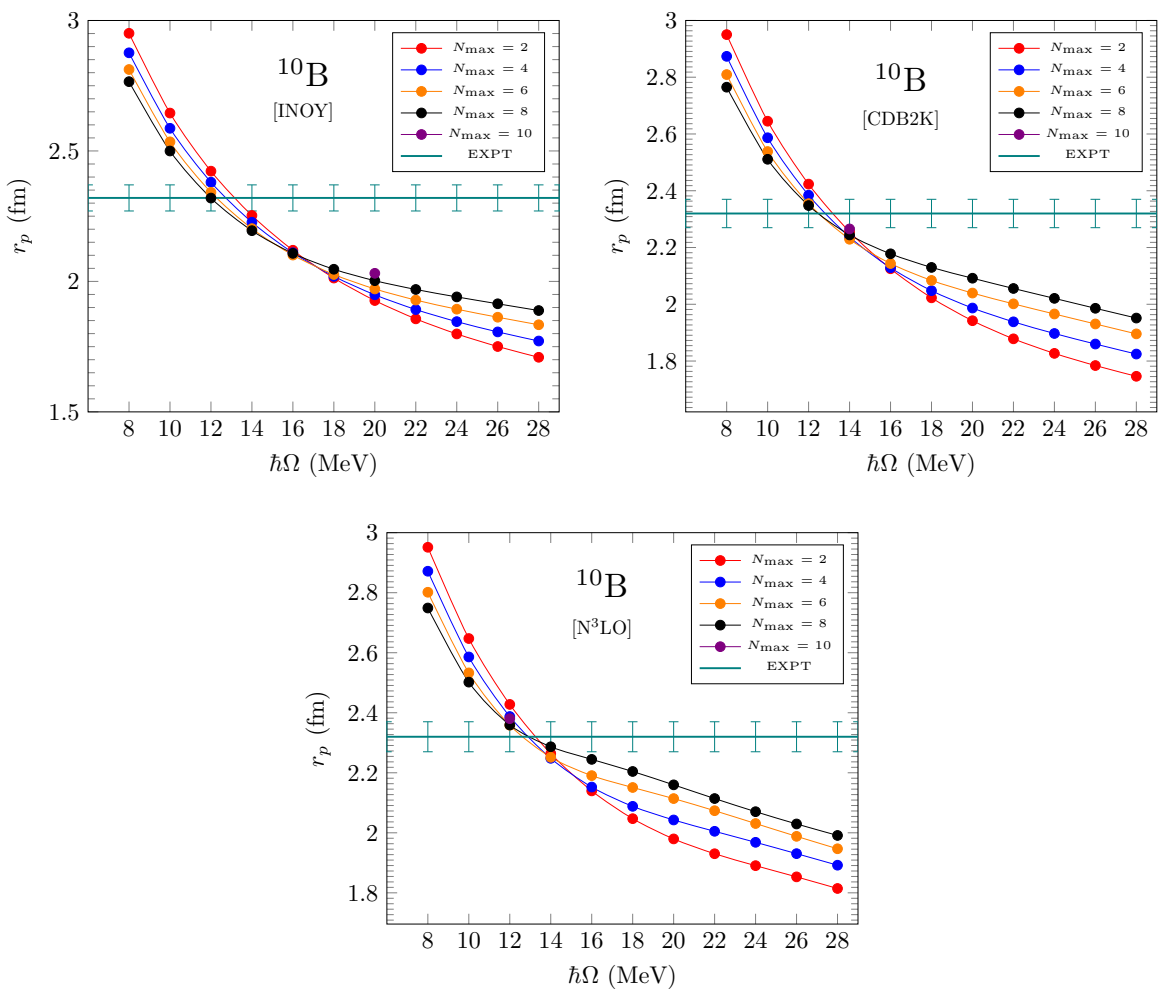

FIG. 8. Variation of r_p of ^{10}B with HO frequency for $N_{\max} = 2$ to 10, corresponding to the INOY, N^{3}LO, and CDB2K interactions. The horizontal line shows the experimental value with the vertical bars representing uncertainty.

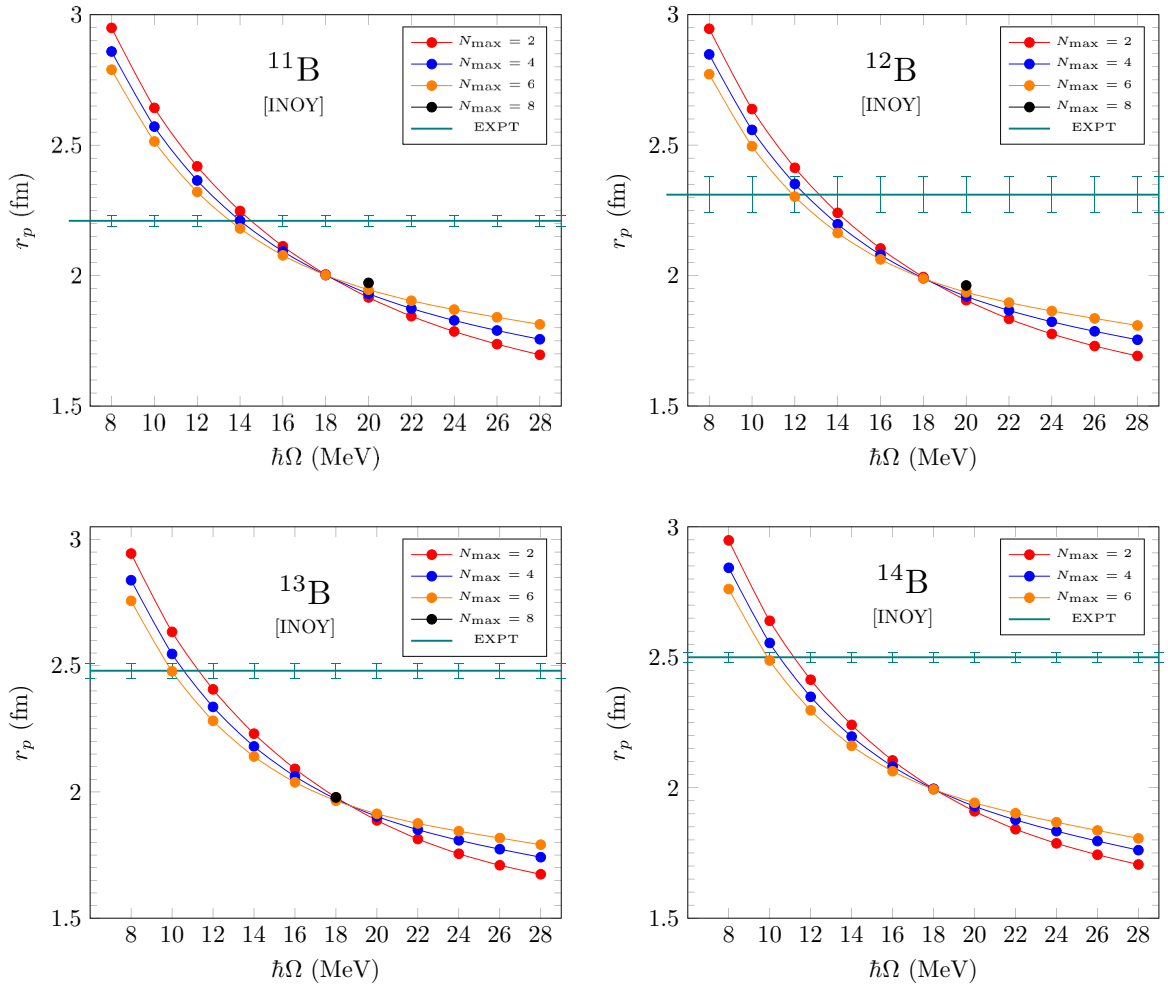

FIG. 9. Variation of r_p of ^{11,12,13,14}B with HO frequency for different $N_{\max}$, corresponding to the INOY interaction. The horizontal line shows the experimental value with the vertical bars representing uncertainty.

interaction in Fig. 9. Obtained r_p values for ^{11}B, ^{12}B, ^{13}B, and ^{14}B are 2.00, 1.99, 1.95, and 1.99 fm, respectively. However, even with this determination of the radii, the experimental trend is not reproduced.

We can conclude that the CDB2K and N^{3}LO interactions give radii which are much closer to experimental value than the radii obtained with the INOY interaction. To some extent this is not surprising given the fact that those interactions underbind the studied isotopes. We have obtained different optimal frequencies for the energy spectra and the point-proton radii. Similar findings were reported for ^{12}C using Daejeon16 and JISP16 interactions in Ref. [46].

VII. CONCLUSIONS

In this work, we have applied the *ab initio* no-core shell model to obtain spectroscopic properties of boron isotopes using INOY, CDB2K, N^{3}LO, and N^{2}LO$_{opt}$ nucleon-nucleon interactions. We have calculated low-lying spectra and other observables with all four interactions and, in addition, compared the NCSM results with shell model using the YSOX valence-space effective interaction. We were able to correctly reproduce the g.s. spin of ^{10}B only with the INOY *NN* interaction. Overall, the INOY interaction reproduced quite reasonably g.s. energies of all the studied isotopes, $^{10-14}$B.

Considering electromagnetic properties, we have obtained fast convergence for $M1$ values, whereas converging $E2$ observables is a computational challenge. The INOY interaction again appears to do better than the other interactions in the reproduction of the $M1$ observables for all isotopes.

Concerning proton radii, we find that the optimal frequency obtained from the minima of the g.s. energy curves and that obtained from the intersection of radii curves could be different. In this case, the CDB2K and N^{3}LO interactions give radii which are much closer to experimental values than the radii obtained with the INOY interaction.

The present study confirms that nonlocality in the *NN* interaction can account for some of the many-nucleon force effects. A nonlocal *NN* interaction such as INOY can provide a quite reasonable description of ground-state energies, excitation spectra, and selected electromagnetic properties, e.g., magnetic moments and $M1$ transitions. However, the description of nuclear radii and consequently of the density remains unsatisfactory. Recent studies show that the inclusion of the $3N$ interaction, in particular $3N$ interaction with nonlocal

regulators, is essential for a correct simultaneous description of nuclear binding and nuclear size [39,84,85].

ACKNOWLEDGMENTS

We would like to thank Christian Forssén for making available the PANTOINE code. We thank Toshio Suzuki for the YSOX interaction. P.C. acknowledges financial support from MHRD (Government of India) for her Ph.D. thesis work. P.C.S. acknowledges a research grant from SERB (India), CRG/2019/000556. P.N. acknowledges support from the NSERC Grant No. SAPIN-2016-00033. TRIUMF receives federal funding via a contribution agreement with the National Research Council of Canada.

[1] B. A. Brown, The nuclear shell model towards the drip lines, Prog. Part. Nucl. Phys. **47**, 517 (2001).
[2] S. Cohen and D. Kurath, Effective interactions for the $1p$ shell, Nucl. Phys. **73**, 1 (1965).
[3] B. A. Brown and W. A. Richter, New USD Hamiltonians for the *sd* shell, Phys. Rev. C **74**, 034315 (2006).
[4] M. Honma, T. Otsuka, B. A. Brown, and T. Mizusaki, Shell-model description of neutron-rich pf-shell nuclei with a new effective interaction GXPF1, Eur. Phys. J. A **25**, 499 (2005).
[5] O. Sorlin and M.-G. Porquet, Nuclear magic numbers: New features far from stability, Prog. Part. Nucl. Phys. **61**, 602 (2008).
[6] T. Otsuka, A. Gade, O. Sorlin, T. Suzuki, and Y. Utsuno, Evolution of shell structure in exotic nuclei, Rev. Mod. Phys. **92**, 015002 (2020).
[7] M. Thoennessen, Current status and future potential of nuclide discoveries, Rep. Prog. Phys. **76**, 056301 (2013).
[8] D. S. Ahn, N. Fukuda, H. Geissel, N. Inabe, N. Iwasa, T. Kubo, K. Kusaka, D. J. Morrissey, D. Murai, T. Nakamura *et al.*, Location of the Neutron Dripline at Fluorine and Neon, Phys. Rev. Lett. **123**, 212501 (2019).
[9] M. Freer, H. Fujita, Z. Buthelezi, J. Carter, R. W. Fearick, S. V. Förtsch, R. Neveling, S. M. Perez, P. Papka, F. D. Smit *et al.*, Cluster structure of ^{12}C and ^{11}Be, Nucl. Phys. A **834**, 621 (2010).
[10] I. Tanihata, Neutron halo nuclei, J. Phys. G: Nucl. Part. Phys. **22**, 157 (1996).
[11] R. Machleidt and D. R. Entem, Chiral effective field theory and nuclear forces, Phys. Rep. **503**, 1 (2011).
[12] E. Epelbaum, H.-W. Hammer, and Ulf-G. Meißner, Modern theory of nuclear forces, Rev. Mod. Phys. **81**, 1773 (2009).
[13] S. Weinberg, Phenomenological Lagrangians, Physica A **96**, 327 (1979).
[14] S. Weinberg, Nuclear forces from chiral Lagrangians, Phys. Lett. B **251**, 288 (1990).
[15] S. Weinberg, Effective chiral lagrangians for nucleon-pion interactions and nuclear forces, Nucl. Phys. B **363**, 3 (1991).
[16] S. Scherer, Introduction to chiral perturbation theory, in *Advances in Nuclear Physics*, Vol. 27, edited by J. W. Negele and E. W. Vogt (Springer, Boston, MA, 2003), pp. 277–538.
[17] W. Leidemann and G. Orlandini, Modern *ab initio* approaches and applications in few-nucleon physics with $A \geqslant 4$, Prog. Part. Nucl. Phys. **68**, 158 (2013).
[18] K. Hebeler, J. D. Holt, J. Menéndez, and A. Schwenk, Nuclear forces and their impact on neutron-rich nuclei and neutron-rich matter, Annu. Rev. Nucl. Part. Sci. **65**, 457 (2015).
[19] S. R. Stroberg, H. Hergert, S. K. Bogner, and J. D. Holt, Nonempirical interactions for the nuclear shell model: An update, Annu. Rev. Nucl. Part. Sci. **69**, 307 (2019).
[20] D. C. Zheng, J. P. Vary, and B. R. Barrett, Large-space shell-model calculations for light nuclei, Phys. Rev. C **50**, 2841 (1994).
[21] P. Navrátil and B. R. Barrett, No-core shell-model calculations with starting-energy-independent multivalued effective interactions, Phys. Rev. C **54**, 2986 (1996).
[22] P. Navrátil and B. R. Barrett, Large-basis shell-model calculations for p-shell nuclei, Phys. Rev. C **57**, 3119 (1998).
[23] P. Navrátil and B. R. Barrett, Four-nucleon shell-model calculations in a Faddeev-like approach, Phys. Rev. C **59**, 1906 (1999).
[24] P. Navrátil, J. P. Vary, and B. R. Barrett, Properties of ^{12}C in the *Ab Initio* Nuclear Shell Model, Phys. Rev. Lett. **84**, 5728 (2000).
[25] P. Navrátil, G. P. Kamuntavičius, and B. R. Barrett, Few-nucleon systems in a translationally invariant harmonic oscillator basis, Phys. Rev. C **61**, 044001 (2000).
[26] P. Navrátil, J. P. Vary and B. R. Barrett, Large-basis *ab initio* no-core shell model and its application to ^{12}C, Phys. Rev. C **62**, 054311 (2000).
[27] P. Navrátil, S. Quaglioni, I. Stetcu, and B. R. Barrett, Recent developments in no-core shell-model calculations, J. Phys. G: Nucl. Part. Phys. **36**, 083101 (2009).
[28] P. Maris, J. P. Vary, and A. M. Shirokov, *Ab initio* no-core full configuration calculations of light nuclei, Phys. Rev. C **79**, 014308 (2009).
[29] B. R. Barrett, P. Navrátil, and J. P. Vary, *Ab initio* no core shell model, Prog. Part. Nucl. Phys. **69**, 131 (2013).
[30] I. Stetcu, B. R. Barrett, P. Navrátil, and J. P. Vary, Long- and short-range correlations in the *ab initio* no-core shell model, Phys. Rev. C **73**, 037307 (2006).
[31] I. Stetcu, B. R. Barrett, P. Navrátil, and J. P. Vary, Effective operators within the *ab initio* no-core shell model, Phys. Rev. C **71**, 044325 (2005).
[32] P. Navrátil and W. E. Ormand, *Ab Initio* Shell Model Calculations with Three-Body Effective Interactions for p-Shell Nuclei, Phys. Rev. Lett. **88**, 152502 (2002).
[33] C. Yuan, T. Suzuki, T. Otsuka, F. Xu, and N. Tsunoda, Shell-model study of boron, carbon, nitrogen, and oxygen isotopes with a monopole-based universal interaction, Phys. Rev. C **85**, 064324 (2012).
[34] T. Myo, A. Umeya, H. Toki, and K. Ikeda, Structures in ^{9,10}Be and ^{10}B studied with the tensor-optimized shell model, Prog. Theor. Exp. Phys. **2015**, 063D03 (2015).
[35] B. S. Pudliner, V. R. Pandharipande, J. Carlson, S. C. Pieper, and R. B. Wiringa, Quantum Monte Carlo calculations of nuclei with $A \leqslant 7$, Phys. Rev. C **56**, 1720 (1997).
[36] D. R. Thompson, M. Lemere, and Y. C. Yang, Systematic investigation of scattering problems with the resonating-group method, Nucl. Phys. A **286**, 53 (1977).

[37] P. Navrátil, V. G. Gueorguiev, J. P. Vary, W. E. Ormand, and A. Nogga, Structure of $A = 10$–13 Nuclei with Two- Plus Three-Nucleon Interactions from Chiral Effective Field Theory, Phys. Rev. Lett. **99**, 042501 (2007).

[38] P. Navrátil and E. Caurier, Nuclear structure with accurate chiral perturbation theory nucleon-nucleon potential: Application to ^{6}Li and ^{10}B, Phys. Rev. C **69**, 014311 (2004).

[39] T. Hüther, K. Vobig, K. Hebeler, R. Machleidt, and R. Roth, Family of chiral two-plus three-nucleon interactions for accurate nuclear structure studies, Phys. Lett. B **808**, 135651 (2020).

[40] E. Epelbaum, H. Krebs, and U.-G. Meißner, Precision Nucleon-Nucleon Potential at Fifth Order in the Chiral Expansion, Phys. Rev. Lett. **115**, 122301 (2015).

[41] P. Maris, *Ab initio* calculations of *p*-shell nuclei up to N^{2}LO in chiral effective field theory, J. Phys.: Conf. Ser. **1291**, 012005 (2019).

[42] A. Ekström, G. Baardsen, C. Forssén, G. Hagen, M. Hjorth-Jensen, G. R. Jansen, R. Machleidt, W. Nazarewicz, T. Papenbrock, J. Sarich *et al.*, Optimized Chiral Nucleon-Nucleon Interaction at Next-to-Next-to-Leading Order, Phys. Rev. Lett. **110**, 192502 (2013).

[43] T. Fukui, L. De Angelis, Y. Z. Ma, L. Coraggio, A. Gargano, N. Itaco, and F. R. Xu, Realistic shell-model calculations for *p*-shell nuclei including contributions of a chiral three-body force, Phys. Rev. C **98**, 044305 (2018).

[44] E. Caurier, P. Navrátil, W. E. Ormand, and J. P. Vary, *Ab initio* shell model for $A = 10$ nuclei, Phys. Rev. C **66**, 024314 (2002).

[45] S. C. Pieper, K. Varga, and R. B. Wiringa, Quantum Monte Carlo calculations of $A = 9$, 10 nuclei, Phys. Rev. C **66**, 044310 (2002).

[46] A. M. Shirokov, I. J. Shin, Y. Kim, M. Sosonkina, P. Maris, and J. P. Vary, N^{3}LO *NN* interaction adjusted to light nuclei in *ab exitu* approach, Phys. Lett. B **761**, 87 (2016).

[47] R. F. Garcia Ruiz, M. L. Bissell, K. Blaum, A. Ekström, N. Frömmgen, G. Hagen, M. Hammen, K. Hebeler, J. D. Holt, G. R. Jansen *et al.*, Unexpectedly large charge radii of neutron-rich calcium isotopes, Nat. Phys. **12**, 594 (2016).

[48] I. Tanihata, T. Kobayashi, O. Yamakawa, S. Shimoura, K. Ekuni, K. Sugimoto, N. Takahashi, T. Shimoda and H. Sato, Measurement of interaction cross sections using isotope beams of Be and B and isospin dependence of the nuclear radii, Phys. Lett. B **206**, 592 (1988).

[49] A. Estradé, R. Kanungo, W. Horiuchi, F. Ameil, J. Atkinson, Y. Ayyad, D. Cortina-Gil, I. Dillmann, A. Evdokimov, F. Farinon *et al.*, Proton radii of $^{12–17}$B Define a Thick Neutron Surface in ^{17}B, Phys. Rev. Lett. **113**, 132501 (2014).

[50] S. Bagchi, R. Kanungo, W. Horiuchi, G. Hagen, T. D. Morris, S. R. Stroberg, T. Suzuki, F. Ameil, J. Atkinson, Y. Ayyad *et al.*, Neutron skin and signature of the $N = 14$ shell gap found from measured proton radii of $^{17–22}$N, Phys. Lett. B **790**, 251 (2019).

[51] P. Doleschall and I. Borbély, Properties of the nonlocal *NN* interactions required for the correct triton binding energy, Phys. Rev. C **62**, 054004 (2000).

[52] D. R. Entem and R. Machleidt, Accurate charge-dependent nucleon-nucleon potential at fourth order of chiral perturbation theory, Phys. Rev. C **68**, 041001(R) (2003).

[53] R. Machleidt, High-precision, charge-dependent Bonn nucleon-nucleon potential, Phys. Rev. C **63**, 024001 (2001).

[54] S. Ôkubo, Diagonalization of Hamiltonian and Tamm-Dancoff equation, Prog. Theor. Phys. **12**, 603 (1954).

[55] K. Suzuki and S. Y. Lee, Convergent theory for effective interaction in nuclei, Prog. Theor. Phys. **64**, 2091 (1980).

[56] K. Suzuki, Construction of Hermitian effective interaction in nuclei: General relation between Hermitian and non-Hermitian forms, Prog. Theor. Phys. **68**, 246 (1982).

[57] K. Suzuki and R. Okamoto, Effective interaction theory and unitary-model-operator approach to nuclear saturation problem, Prog. Theor. Phys. **92**, 1045 (1994).

[58] S. K. Bogner, R. J. Furnstahl, and R. J. Perry, Similarity renormalization group for nucleon-nucleon interactions, Phys. Rev. C **75**, 061001(R) (2007).

[59] E. D. Jurgenson, P. Navrátil, and R. J. Furnstahl, Evolving nuclear many-body forces with the similarity renormalization group, Phys. Rev. C **83**, 034301 (2011).

[60] C. Forssén, P. Navrátil, W. E. Ormand, and E. Caurier, Large basis *ab initio* shell model investigation of ^{9}Be and ^{11}Be, Phys. Rev. C **71**, 044312 (2005).

[61] E. Caurier and P. Navrátil, Proton radii of ^{4,6,8}He isotopes from high-precision nucleon-nucleon interactions, Phys. Rev. C **73**, 021302(R) (2006).

[62] C. Forssén, E. Caurier, and P. Navrátil, Charge radii and electromagnetic moments of Li and Be isotopes from the *ab initio* no-core shell model, Phys. Rev. C **79**, 021303(R) (2009).

[63] C. Forssén, R. Roth, and P. Navrátil, Systematics of 2^{+} states in C isotopes from the no-core shell model, J. Phys. G: Nucl. Part. Phys. **40**, 055105 (2013).

[64] E. D. Jurgenson, P. Maris, R. J. Furnstahl, P. Navrátil, W. E. Ormand, and J. P. Vary, Structure of *p*-shell nuclei using three-nucleon interactions evolved with the similarity renormalization group, Phys. Rev. C **87**, 054312 (2013).

[65] D. H. Gloeckner and R. D. Lawson, Spurious center-of-mass motion, Phys. Lett. B **53**, 313 (1974).

[66] S. Baroni, P. Navrátil, and S. Quaglioni, *Ab Initio* Description of the Exotic Unbound ^{7}He Nucleus, Phys. Rev. Lett. **110**, 022505 (2013).

[67] A. Calci, P. Navrátil, R. Roth, J. Dohet-Eraly, S. Quaglioni, and G. Hupin, Can *Ab Initio* Theory Explain the Phenomenon of Parity Inversion in ^{11}Be?, Phys. Rev. Lett. **117**, 242501 (2016).

[68] P. Doleschall, I. Borbély, Z. Papp, and W. Plessas, Nonlocality in the nucleon-nucleon interaction and three-nucleon bound states, Phys. Rev. C **67**, 064005 (2003).

[69] P. Doleschall, Influence of the short range nonlocal nucleon-nucleon interaction on the elastic *n-d* scattering: Below 30 MeV, Phys. Rev. C **69**, 054001 (2004).

[70] R. Machleidt, F. Sammarruca, and Y. Song, Nonlocal nature of the nuclear force and its impact on nuclear structure, Phys. Rev. C **53**, R1483(R) (1996).

[71] R. Machleidt, K. Holinde, and Ch. Elster, The Bonn meson-exchange model for the nucleon-nucleon interaction, Phys. Rep. **149**, 1 (1987).

[72] R. Machleidt, The meson theory of nuclear forces and nuclear structure, Adv. Nucl. Phys. **19**, 189 (1989).

[73] D. Logoteta, Optimized chiral N^{2}LO interactions in nuclear matter, Eur. Phys. J. A **54**, 111 (2018).

[74] R. B. Wiringa, V. G. J. Stoks, and R. Schiavilla, Accurate nucleon-nucleon potential with charge-independence breaking, Phys. Rev. C **51**, 38 (1995).

[75] E. Caurier and F. Nowacki, Present status of shell model techniques, Acta Phys. Pol. B **30**, 705 (1999).

[76] E. Caurier, G. Martínez-Pinedo, F. Nowacki, A. Poves, and A. P. Zuker, The shell model as a unified view of nuclear structure, Rev. Mod. Phys. **77**, 427 (2005).

[77] C. Forssén, B. D. Carlsson, H. T. Johansson, D. Sääf, A. Bansal, G. Hagen, and T. Papenbrock, Large-scale exact diagonalizations reveal low-momentum scales of nuclei, Phys. Rev. C **97**, 034328 (2018).

[78] N. Shimizu, T. Mizusaki, Y. Utsuno, and Y. Tsunoda, Thick-restart block Lanczos method for large-scale shell-model calculations, Comput. Phys. Commun. **244**, 372 (2019).

[79] A. Saxena and P. C. Srivastava, *Ab initio* no-core shell model study of neutron-rich nitrogen isotopes, Prog. Theor. Exp. Phys. **2019**, 073D02 (2019).

[80] A. Saxena and P. C. Srivastava, *Ab initio* no-core shell model study of $^{18-23}$O and $^{18-24}$F isotopes, J. Phys. G: Nucl. Part. Phys. **47**, 055113 (2020).

[81] Data extracted using the NNDC World Wide Web site from the ENSDF, https://www.nndc.bnl.gov/ensdf/.

[82] IAEA, https://www-nds.iaea.org/nuclearmoments/.

[83] M. A. Caprio, P. Maris, and J. P. Vary, Halo nuclei ^{6}He and ^{8}He with the Coulomb-Sturmian basis, Phys. Rev. C **90**, 034305 (2014).

[84] A. Ekström, G. R. Jansen, K. A. Wendt, G. Hagen, T. Papenbrock, B. D. Carlsson, C. Forssén, M. Hjorth-Jensen, P. Navrátil, and W. Nazarewicz, Accurate nuclear radii and binding energies from a chiral interaction, Phys. Rev. C **91**, 051301(R) (2015).

[85] V. Somà, P. Navrátil, F. Raimondi, C. Barbieri, and T. Duguet, Novel chiral Hamiltonian and observables in light and medium-mass nuclei, Phys. Rev. C **101**, 014318 (2020).